227 (2023) 211952

Contents lists available at ScienceDirect

Geoenergy Science and Engineering

journal homepage: www.sciencedirect.com/journal/geoenergy-science-and-engineering

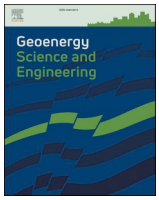

A novel method for seismic-attribute optimization driven by forward modeling and machine learning in prediction of fluvial reservoirs

Wei Li [a,b], Dali Yue [a,b,*], Luca Colombera [c,d], Dongping Duan [e], Tao Long [f], Shenghe Wu [a,b], Yuming Liu [a,b]

[a] State Key Laboratory of Petroleum Resources and Prospecting, China University of Petroleum (Beijing), Beijing, 102249, China
[b] College of Geosciences, China University of Petroleum (Beijing), Beijing, 102249, China
[c] Dipartimento di Scienze Della Terra e Dell'Ambiente, Università Degli Studi di Pavia, Via Ferrata 1, 27100, Pavia, Italy
[d] Fluvial, Eolian & Shallow-Marine Research Group, School of Earth & Environment, University of Leeds, Leeds, LS2 9JT, UK
[e] Shanghai Branch of CNOOC (China) Ltd., Shanghai, 200335, China
[f] SINOPEC Exploration Company, Chengdu, Sichuan, 610041, China

ARTICLE INFO

Keywords:
Seismic attribute
Forward seismic modeling
Supervised learning
Sand thickness
Channel belt

ABSTRACT

The use of seismic attributes for hydrocarbon exploration is well established, and the integration of multiple attributes by supervised machine learning is increasingly being applied as an effective method for attribute optimization. However, this method relies upon a dense array of wells to be employed as a training dataset, which limits its application to fields with sparse boreholes, especially offshore. To address this limitation, this study proposes a novel method of seismic attribute integration driven by forward seismic modeling, enabling the integration of multiple attributes by supervised learning in fields with a limited number of wells. This proposed method consists of two main tasks: (i) establishing a forward geological (lithological) model on a well-correlation section by forward seismic modeling, based on seismic data and wells from the study area; (ii) fusing multiple seismic attributes by supervised machine learning, employing the forward geological model and its synthetic seismic reflection as the training dataset. This method is applied and tested on a real-world case study from the East China Sea region. In this case study, seismic surface attributes of root-mean-square amplitude, max peak amplitude and sweetness are selected and then integrated using the proposed method. The integrated seismic attribute shows significant advantages for the detection of channel belts. Notably, it results in markedly improved correlation between seismic attribute and sand thickness, with the correlation coefficient increasing from 0.586 to 0.849, compared to the original seismic attribute.

1. Introduction

The use of seismic attributes for hydrocarbon exploration and reservoir characterization is well established, with extensively documented applications to the identification of thin beds, faults, and hydrocarbon sweet spots (Chopra and Marfurt, 2005; Hosseinyar et al., 2019; McArdle et al., 2014). Extensive research has been devoted to the improvement of the resolution and reliability of seismic attributes, which falls in two different strands: (i) derivation of new attributes by means of dedicated algorithms (Chopra and Marfurt, 2005; Hart, 2008; Zhang et al., 2014), and (ii) development of new workflows and multivariable algorithms for utilizing multiple existing attributes (Li et al., 2019a; McArdle et al., 2014; Yue et al., 2019). More than one hundred of seismic attributes have been developed in the past forty years, but only a few attributes have been developed in recent years that show significant advantages in the identification of thin beds and sweet spots, compared to established ones (Chopra and Marfurt, 2005; Li et al., 2020; Mahob and Castagna, 2003; Shao et al., 2021). On the other hand, a series of case studies has shown that the integration of multiple existing seismic attributes with new comprehensive workflows holds promise as a predictive approach (La Marca and Bedle, 2022; Naseer and Asim, 2017; Wang et al., 2017). Therefore, research on improved attribute integration has received special attention, and recent work on the integration of multiple seismic attributes by machine learning with a supervised algorithm has particularly improved seismic interpretation (Anifowose et al., 2019; Li et al., 2020, 2021; Sediek et al., 2022; Yue

* Corresponding author. State Key Laboratory of Petroleum Resources and Prospecting, China University of Petroleum (Beijing), Beijing, 102249, China.
E-mail addresses: wei_li@cup.edu.cn (W. Li), yuedali@cup.edu.cn (D. Yue).

https://doi.org/10.1016/j.geoen.2023.211952
Received 26 February 2023; Received in revised form 17 May 2023; Accepted 26 May 2023
Available online 29 May 2023

et al., 2019; Zheng et al., 2022a, 2022b). However, this type of method requires a large amount of well-log data to be used as a training dataset, from which the algorithm can learn. Such methods are therefore only suitable for areas in which dense arrays of wells are present, which greatly limits its application and popularization.

Forward seismic modeling is a forward modeling technique applied to simulate the seismic reflection of geological models, by means of different synthetic algorithms (Hilterman, 1975; Tomasso et al., 2010), which has been widely applied in the identification of sequence stratigraphic features, structural features, thin beds and sedimentary facies (Armitage and Stright, 2010; Bakke et al., 2013; Eichelberger et al., 2017; Tomasso et al., 2010; Yue et al., 2019). It is generally argued, however, that forward seismic modeling should be based on real-world geological observations for it to act as a sound basis for guiding seismic interpretation (Bakke et al., 2013; Hilterman, 1975; Li et al., 2019b; Stright et al., 2014). Therefore, the outputs of forward seismic modeling based on well and seismic data may provide a training dataset for seismic interpretation in areas with limited wells (Bakke et al., 2013; Eichelberger et al., 2017; Tomasso et al., 2010; Yue et al., 2019), by enabling the integration of multiple seismic attributes with supervised machine learning.

The aim of this study is to develop a novel method for seismic-attribute optimization that leverages forward seismic modeling and machine learning algorithms. By achieving this aim, we will be able to: (i) overcome inherent limitations in intelligent integration of multiple seismic attributes with machine learning, i.e., its need for a dense well dataset; and (ii) to broaden the scope of this approach to fields with limited numbers of wells.

2. Geological setting

The study area lies in the Xihu Sag, the East China Sea shelf basin. The Xihu Sag is a Meso-Cenozoic sedimentary basin, which is bounded to the west by the Central Uplift Group, to the east by the Taiwan-Sinzi Fold Belt, to the north by the Fujiang Sag, and to the south by the Diaobei Sag (Fig. 1a) (Hao et al., 2018). The stratigraphic interval of interest is part of the Huagang Formation (Paleogene, Cenozoic) (Fig. 1b), which is interpreted as a fluvial succession deposited by braided rivers and braided-river deltas (Xu et al., 2020; Zhou et al., 2020). This target interval includes four reservoir zones, ranging in thickness from 35 m to 60 m (Fig. 1b). The depth of the interval ranges from 2900 m to 3500 m.

3. Dataset and methodology

This research develops a novel method for seismic-attribute optimization driven by forward seismic modeling, in which the selection of seismic attributes and tools of the forward seismic modeling and spectral decomposition were used. Hence, the integrated workflow, spectral decomposition, forward seismic modeling, and selection of seismic attributes are detailed in this section.

3.1. Dataset

There are 11 wells in the study area; W1, W2 and W3 are vertical wells, whereas the others are deviated wells. These wells are concentrated around a drilling platform, and as such most of the field area is not covered by drilled wells (Fig. 2a). Therefore, integration of multiple

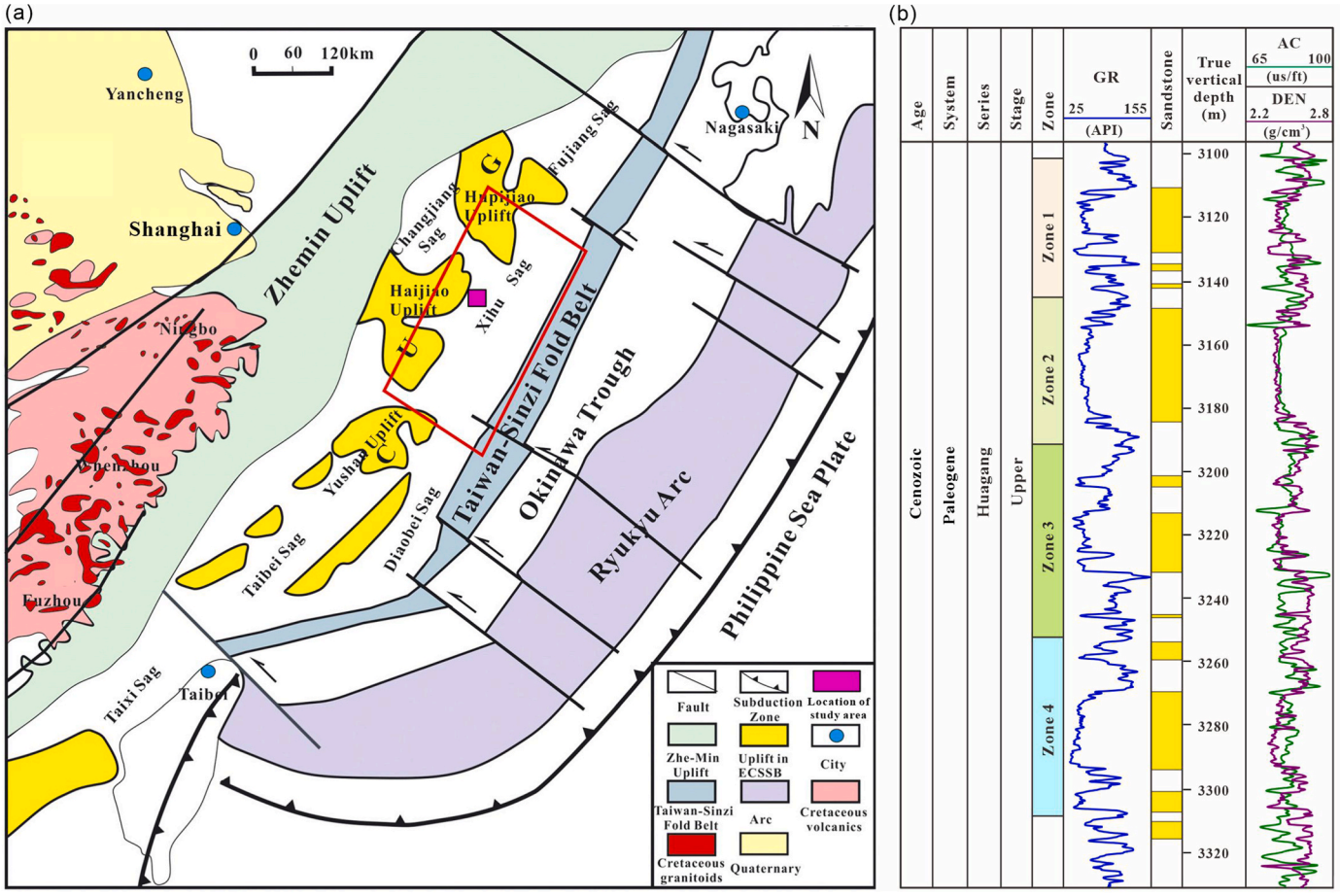

Fig. 1. (A) Tectonic framework of the East China Sea area (modified after Hao et al., 2018). The red box highlights the Xihu Sag. Abbreviation: ECSSB – the East China Sea Shelf Basin, WDG – the West Depression Group, CUG – the Central Uplift Group, WDG – the East Depression Group. (b) Profile of well W1 in the Huagang Formation of Paleogene, showing the lithological section and wireline logs of GR, AC and DEN. Abbreviation: GR – gamma ray, AC – acoustic, DEN – density.

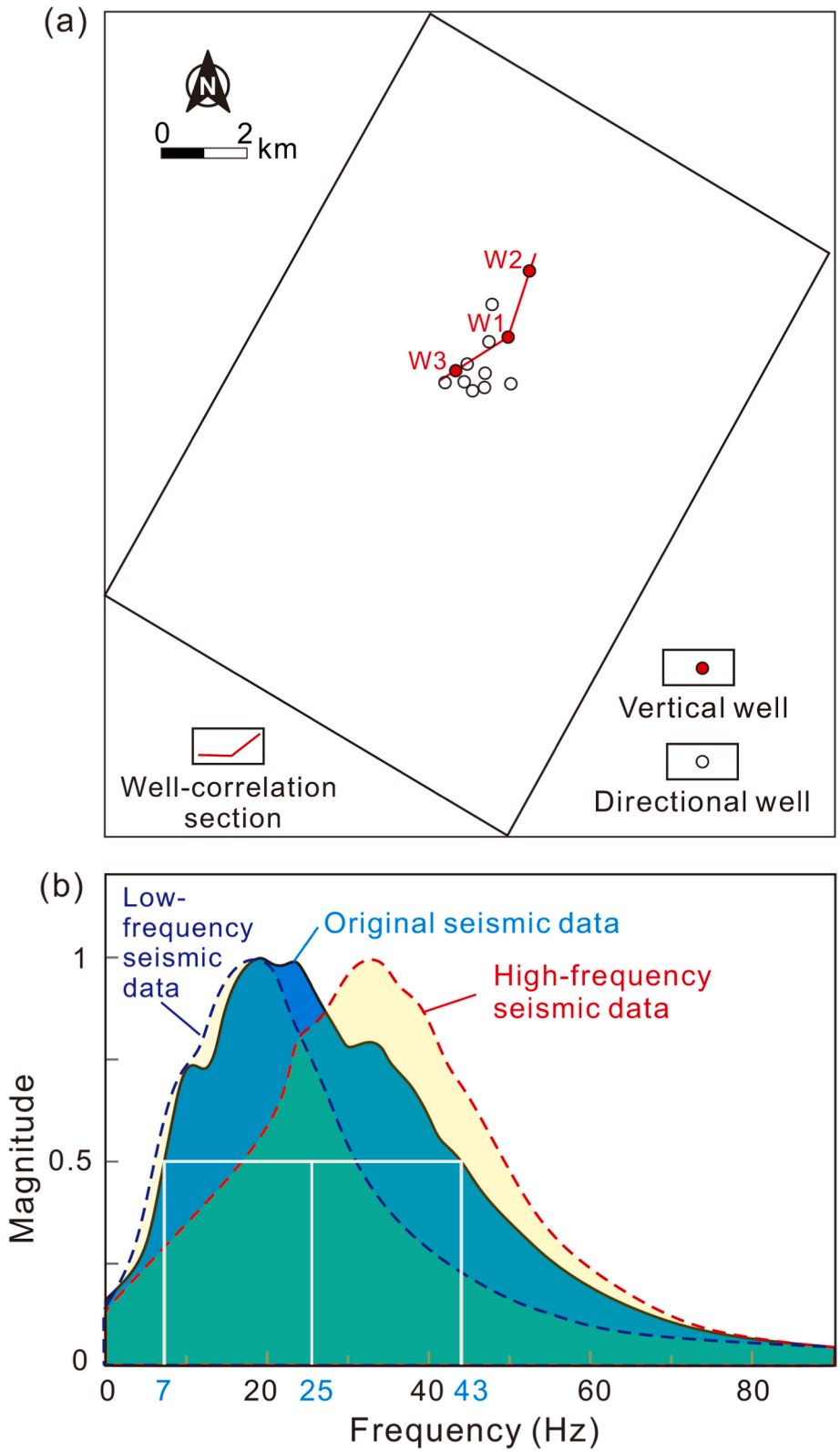

Fig. 2. (A) Map showing the study area and the well location. (b) Normalized spectra of original, low-frequency and high-frequency spectral-decomposed seismic data.

seismic attributes with supervised machine learning is difficult because the sparse wells cannot provide a significant supervised training dataset. All the wells have wireline logs, including gamma ray (GR), acoustic (AC), density (DEN), and deep and shallow laterologs (LLD and LLS). The study area is covered with a 3D seismic cube, with an effective bandwidth of 7–43 Hz and a dominant frequency of 25 Hz (Fig. 2b). The inline and crossline spacings are 12.5 m and 25 m, respectively; the vertical sample interval is 2 ms. The seismic data were processed to a normal polarity display. The P-wave velocity of the study interval is between 3800 m/s and 4150 m/s, based on the statistics from the

acoustic wireline logs.

3.2. Integrated workflow of the proposed method

To address the limitation of fusing multiple seismic attributes by machine learning, this research develops a novel method for seismic-attribute optimization that leverages forward seismic modeling and machine learning algorithms. The integrated workflow for this proposed method can be summarized into five main steps: i) spectral decomposition, ii) forward seismic modeling of the real well-correlation section, iii) generation of pseudo-wells, iv) training by machine learning with a supervised algorithm, v) application of the trained model to the actual seismic data (Fig. 3).

The first two steps are detailed in following sections 3.3 and 3.4. The synthetic seismic model in the second step is produced using parameters of the study area, including the lithological model, acoustic impedance features and seismic wavelets, and in such way that it becomes comparable to the real seismic data. Therefore, this forward seismic model provides a suitable training dataset for supervised machine learning. In the third step (Figs. 3c), 100 equally spaced pseudo-wells were extracted from this forward seismic model. Then, machine learning was performed on the dataset of 100 pseudo-wells (Fig. 3d), with common supervised algorithms for relatively small training datasets, including support vector regression (SVR), random forest (RF), genetic neural network

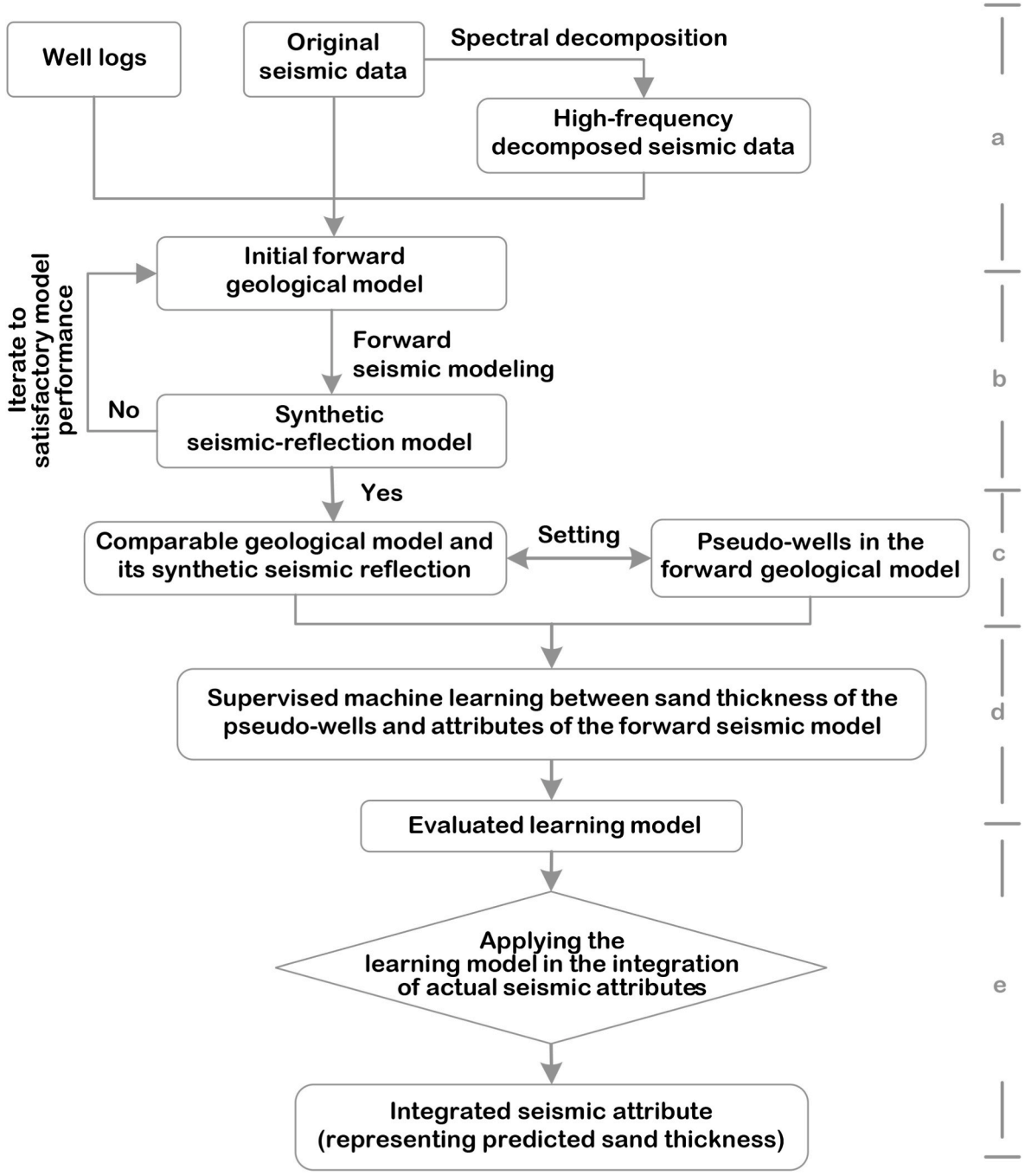

Fig. 3. Integrated workflow diagram outlining the methodology of seismic attribute integration driven by forward seismic modeling and machine learning. There are five steps: a) spectral decomposition, b) forward seismic modeling, c) generation of pseudo-wells, d) training by machine learning, e) application of the trained model to the actual seismic data.

(GNN). Technical aspects of these algorithms were explained in our earlier related articles (Li et al., 2019a, 2021). Machine learning with all the three algorithms produced similar results. This article focuses on results produced by machine learning with a SVR algorithm, in which a radial basis function kernel was used, setting the machine learning as explained in detail by Li et al. (2021). At last, the trained SVR model was applied to integrate the seismic attributes over the study area (Fig. 3e), as conditioned on the 11 wells, to predict sand thicknesses.

3.3. Spectral decomposition

Spectral decomposition is a kind of segregation technique in the frequency domain, which can decompose the seismic amplitude cube into its constituent frequency volumes (Castagna and Sun, 2006; Naseer and Asim, 2017; Partyka et al., 1999). Each frequency cube can benefit the analyses of seismic reflections and reservoir characterization. There are several common techniques for spectral decomposition, in which the continuous wavelet transform (CWT) has been a popular tool (Castagna and Sun, 2006; Partyka et al., 1999; Postnikov et al., 2016; Sinha et al., 2005). The time window of the CWT can adapt to frequency variations in seismic signal. With decreases in frequency, the time window increases and the resolution decreases, i.e. smaller time windows and higher resolutions correspond to the highest frequency data. Thus, the time-variant window can highlight detailed information on varied frequencies (Bitrus et al., 2016; Li et al., 2019a; Postnikov et al., 2016). This tool of CWT is proved to be robust and effective, and has been applied extensively (de Matos et al., 2011; Li et al., 2019b; Naseer and Asim, 2017; Sinha et al., 2005; Zeng, 2017). The original seismic data were decomposed into a relatively low- and high-frequency seismic cubes using the CWT technique and the Marr wavelet (as the mother wavelet). It is important to ensure that the original seismic data have a relatively-narrow effective bandwidth, so that it was merely decomposed into two seismic bands. The low- and high-frequency spectral-decomposed seismic data have a dominant frequency of 19 Hz and 35 Hz, respectively (Fig. 1c). Compared to the low-frequency seismic data, both original and high-frequency seismic data have their own advantages: the former have more information and a higher signal-to-noise ratio, whereas the latter have higher resolution (Armitage and Stright, 2010; Li et al., 2019b; Naseer and Asim, 2017; Tomasso et al., 2010). Therefore, both types of seismic data were employed for establishing the geological forward model.

3.4. Methods of forward seismic modeling

(1) Conceptual geological model

Two simple, conceptual geological models were designed as shown in Fig. 4; these consist of a sandstone wedge in a mudstone background (Fig. 4a), and of a mudstone wedge interbedded with two tabular sandstones, in a mudstone background (Fig. 4b), respectively. According to the scale of channel belts and mudstone interlayer the study area, the thickness of both the sandstone and interbedded mudstone wedges varies between 0 m and 50 m. The two tabular sandbodies in Fig. 3b have a thickness of 25 m, equal to the average thickness of channel-belt sandbodies.

The density and acoustic velocity of sandstone is 2.43 g/cm^3 and 3954 m/s, respectively; those of mudstone are 2.61 g/cm^3 and 4056 m/s, respectively. These values were set based on the statistics from the density and sonic wireline logs (Fig. 1b). Both geological models were convolved to synthesize their seismic-reflection expression, using the statistical wavelets extracted from the original and high-frequency decomposed seismic data (Fig. 4), whose length is 128 ms with a dominant frequency of 25 Hz. Also, a 90° phase shift was applied, in order to obtain a better match between the seismic waveforms and the geobody (Zeng and Backus, 2005).

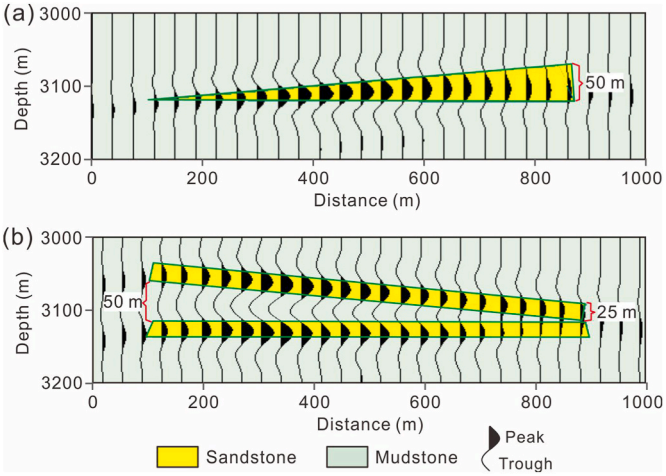

Fig. 4. Conceptual geological models and their synthetic seismic reflections based on forward modeling. The reflections are synthetized using the statistical wavelet extracted from the original seismic data, and are shown in a 90°-phase display. (a) Simple sandstone wedge model. (b) Interbedded sandstone and mudstone wedge model. The velocities of sandstone and mudstone is 3954 m/s and 4056 m/s, respectively; the densities of sandstone and mudstone is 2.43 g/cm^3 and 2.61 g/cm^3, respectively. Forward modeling is based on concept of "wave front sweep velocity" (Hilterman, 1975), and was carried out in GeoGraphix Seismic Modeling.

(2) Forward seismic modeling of well-correlation section

Seismic modeling of the well-correlation section was undertaken in three steps (Fig. 5). First, an initial lithological model was established based on GR logs, and controlled the 90°-phase waveforms of the original and high-frequency seismic data. As shown in Fig. 4, the 90°-phase waveforms are broadly associated with channel sandbodies. For the initial model, channel bodies intersected by the wells were identified using GR logs at first, and such identified channel bodies were then extended to the area between wells based on waveform features of the original and high-frequency seismic data. This geological model was then transformed into an acoustic impedance model using wireline logs of acoustic impedance (density and acoustic). Second, the resulting acoustic impedance model was convolved to obtain a synthetic seismic-reflection model using the statistical wavelet of the original seismic data.

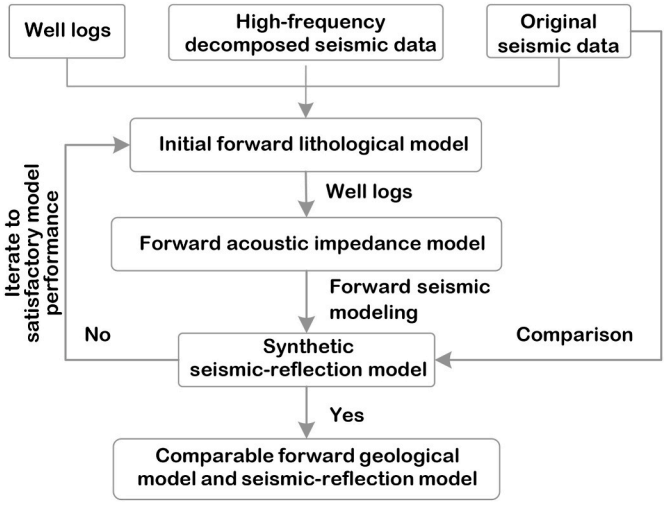

Fig. 5. Workflow diagram outlining the forward seismic modeling of a well-correlation section. There are three main steps, including establishment of an initial lithological model, convolution of the acoustic-impedance model, and iterative adjustment of the synthetic seismic reflections.

Finally, this synthetic seismic model was compared visually to the actual seismic profile on the same well-correlation section. The initial geological model was then adjusted iteratively until the synthetic seismic reflection profile became comparable to the real seismic profile along the well-correlation panel.

3.5. Selection of seismic attributes

The selection of seismic attributes is summarized into three steps. First, 16 types of surface attributes that are commonly used to identify channel sandbodies were calculated in the original seismic data, for each reservoir zone. Second, correlations between surface attributes and sand thickness interpreted from well logs were analyzed. For instance, it was observed that in reservoir zone 2 eight types of seismic attributes show relatively higher Pearson's correlation coefficients (no less than 0.45) with sand thickness (Table 1). These attributes were therefore selected preliminarily. Third, cluster analysis was carried out, and only one kind of attribute would be selected from each cluster to reduce redundant seismic information (see below for details). Similarly, the same types of attributes were selected from the low- and high-frequency spectral-decomposed seismic data.

4. Results

4.1. Seismic attributes

Eight types of seismic attributes were selected preliminarily, according to their correlation with sand thickness interpreted by well logs (Table 1). These attributes were analyzed using a hierarchical cluster algorithm, and were divided into three clusters (Fig. 6). The cluster 1 consists of seismic attributes MPA, APA MA and TA (Table 1; red color in Fig. 6); the cluster 2 includes attributes of RMS, TAA and AAA (Table 1; blue color in Fig. 6); the cluster 3 is the sweetness attribute. A single attribute type was selected from each cluster to reduce redundancy in seismic information. Thus, eventually, attributes MPA, RMS and sweetness were selected based on their correlation with sand thickness (Table 1). Attributes MPA, RMS and sweetness were additionally extracted from the high- and low-frequency dataset. The MPA attributes calculated from original and high-frequency seismic data in reservoir zone 2 are shown in Fig. 7; high-value areas indicate the overall spatial distribution of channel-belt sandbodies. Resolution of low-frequency seismic attributes is too low to detect channel belts, so they are not used in this study. Channel belts outlined by the high-frequency attribute appear as slightly more continuous.

Table 1
Seismic attributes and their Pearson's correlation coefficient with sand thickness. R indicates the Pearson's correlation coefficient. Attributes are ranked in order of decreasing strength in correlation. Correlations are considered statistically significant for P-values less than 0.01.

Names of seismic attributes	R for attribute vs sand thickness	P-value	Names of seismic attributes	R for attribute vs sand thickness	P-value
Max Peak Amplitude (MPA)	0.586	<0.01	Total Energy	0.387	<0.01
Average Peak Amplitude (APA)	0.551	<0.01	Average Peak Frequency	−0.324	<0.01
Root-Mean-Square Amplitude (RMS)	0.548	<0.01	Maximum Trough Amplitude	0.331	<0.01
Total Amplitude (TA)	0.521	<0.01	Instant Frequency Slope	0.304	<0.01
Mean Amplitude (MA)	0.514	<0.01	Average Trough Amplitude	−0.272	0.012
Sweetness	0.491	<0.01	Reflection Strength Slope	−0.154	0.018
Total Absolute Amplitude (TAA)	0.477	<0.01	Average Instant Phrase	−0.118	0.036
Average Absolute Amplitude (AAA)	0.446	<0.01	Average Reflection Strength	0.052	0.034

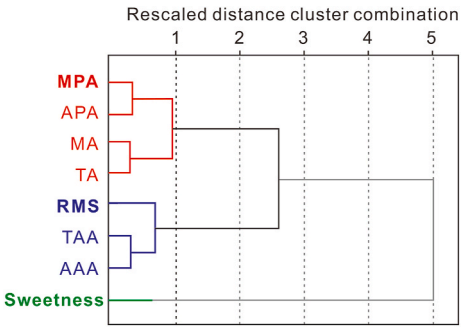

Fig. 6. Dendrogram of the seismic attributes using hierarchical cluster analysis. Clusters 1, 2 and 3 are shown in colors of red, blue and green, respectively. Codes of the seismic attributes are explained in Table 1.

4.2. Forward seismic modeling

(1) Responses of the forward seismic model

The two conceptual forward models (Fig. 4) were convolved to synthetic seismic reflections, using statistical wavelets extracted from the original and high-frequency seismic data (Fig. 8). The synthetic results indicate that channel sandstones are associated with peak reflections, whereas the interbedded mudstone is expressed by a trough reflection, in 90°-phase display. Also, synthetic seismic reflections based on the high-frequency statistical wavelet show a higher resolution, yielding a better match between the geobody and the seismic waveforms (Fig. 8).

4.3. Forward seismic model of a well-correlation section

Generally, original seismic data have a higher signal-to-noise ratio (Fig. 8a and b), whereas high-frequency spectral-decomposed seismic data have higher resolution (Fig. 8c and d) (Armitage and Stright, 2010; Li et al., 2019b; Naseer and Asim, 2017; Tomasso et al., 2010). As detailed in section 2.4 (Fig. 5), an initial forward lithological model was established (Fig. 9c) based on features of well logs and seismic waveforms (Fig. 9a and b). This geological model was then convoluted using the statistical wavelet of the original seismic data, producing a synthetic seismic-reflection model (Fig. 9d). Commonly, the amplitude range in the synthetic seismic profile is similar to that of the actual seismic data, because the used seismic wavelet and acoustic impedance information are based on actual seismic data and well logs. Nonetheless, the amplitude range of the synthetic seismic profile was corrected to match that of the related, actual seismic profile, according to recorded maximum and minimum values. This synthetic model was then compared to the original seismic data on the same well-correlation section (comparison between Fig. 9a and d). As may be expected, significant differences exist between the synthetic and real seismic profile (blue arrows in Fig. 9). Hence, the initial forward geological model was adjusted iteratively (Fig. 9e), until the differences between the synthetic and real seismic profiles became negligible or were deemed acceptable

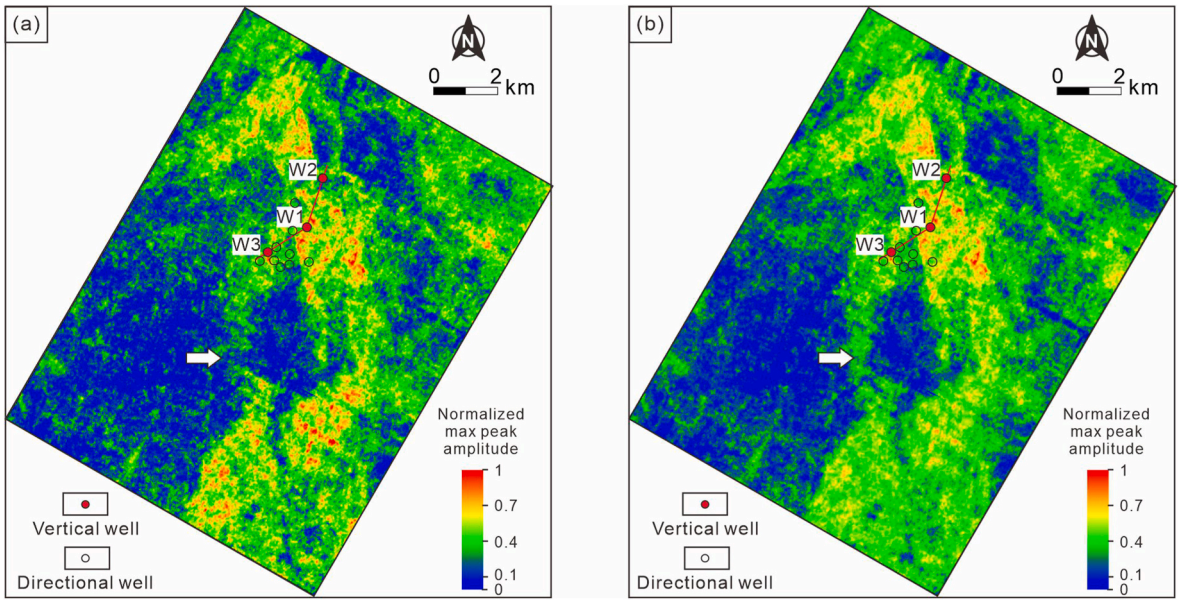

Fig. 7. The MPA attribute of reservoir zone 2, in the study area. (a) Attribute extracted from the original seismic data. (b) Attribute extracted from the high-frequency spectral-decomposed seismic data. The channel belts shown on the both surface attributes are similar approximately, and the arrowed channel belt is slightly clearer in part b.

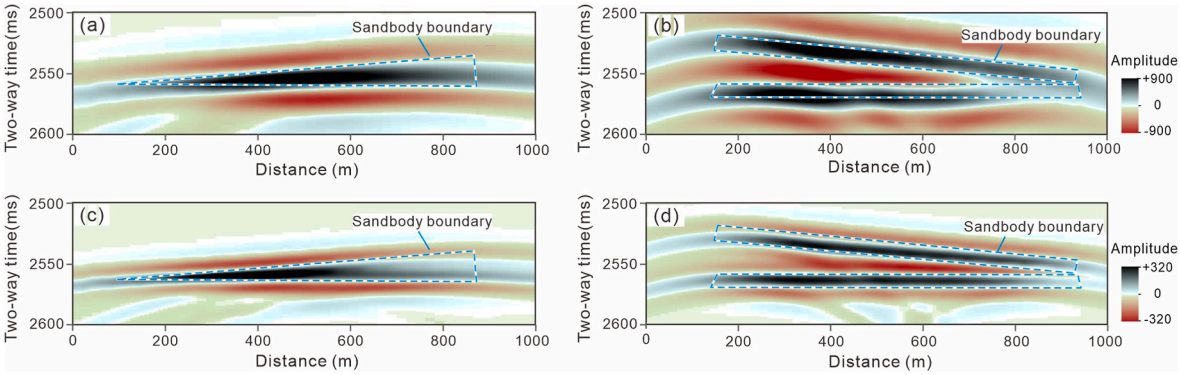

Fig. 8. Synthetic seismic-reflection models, whose lithological models are shown in Fig. 4. (a) and (b) were produced with the original statistical wavelet, showing a dominant frequency of 25 Hz. (c) and (d) were produced with the high-frequency statistical wavelet, showing a dominant frequency of 35 Hz. These synthetic seismic profiles are with a 90°-phase display.

(Fig. 9a and f).

4.4. *Integrated seismic attributes derived from forward seismic modeling*

As explained in section 3.2, a total of 100 pseudo-wells were placed in the adjusted, synthetic seismic-reflection forward model (five wells are displayed in Fig. 9e and f). Sand thickness and seismic attributes of each reservoir zone were then calculated around the pseudo-wells. Afterwards, supervised machine learning with a SVR algorithm was performed between sand thickness and seismic attributes (i.e., MPA, RMS and sweetness attributes, see Fig. 6) of the pseudo-wells, and a trained SVR model was produced. Notably, the actual wells were not used in the supervised machine learning. Lastly, the trained SVR model was applied to integrate the MPA, RMS and sweetness attributes observed over the study area.

Seismic attributes calculated from original and high-frequency seismic data were used, respectively, because of their own advantages as mentioned in section 3.5 (Armitage and Stright, 2010; Li et al., 2019b; Naseer and Asim, 2017; Tomasso et al., 2010). The integrated attribute using original MPA, RMS and sweetness attributes is shown in Fig. 10a, and that using high-frequency MPA, RMS and sweetness attributes is shown in Fig. 10b. The integrated attributes represent predicted sand thickness based on training using the sand thickness of pseudo-wells. Features of the integrated results are similar, showing similar channel belts (Fig. 10a and b).

Channel belts mapped in the integrated attributes are more clearly delineated than those recognized in the original attributes (Figs. 7 and 10). By combining the integrated attributes (Fig. 10b) and well logs (Fig. 10d), the spatial distribution of architectural elements can be reconstructed (Fig. 9c).

5. Discussion

5.1. *Reliability and advantages*

Wells that were not used in the supervised machine learning can be utilized for cross-validation purposes, to evaluate the integrated seismic attributes derived by forward seismic modeling. To this end, correlations are evaluated between the sand thickness observed in actual wells and both the integrated seismic attribute (Fig. 11a, corresponding to Fig. 10a), and the original MPA attribute (Fig. 11b). The high correlation exhibited by the integrated attribute highlights its predictive power

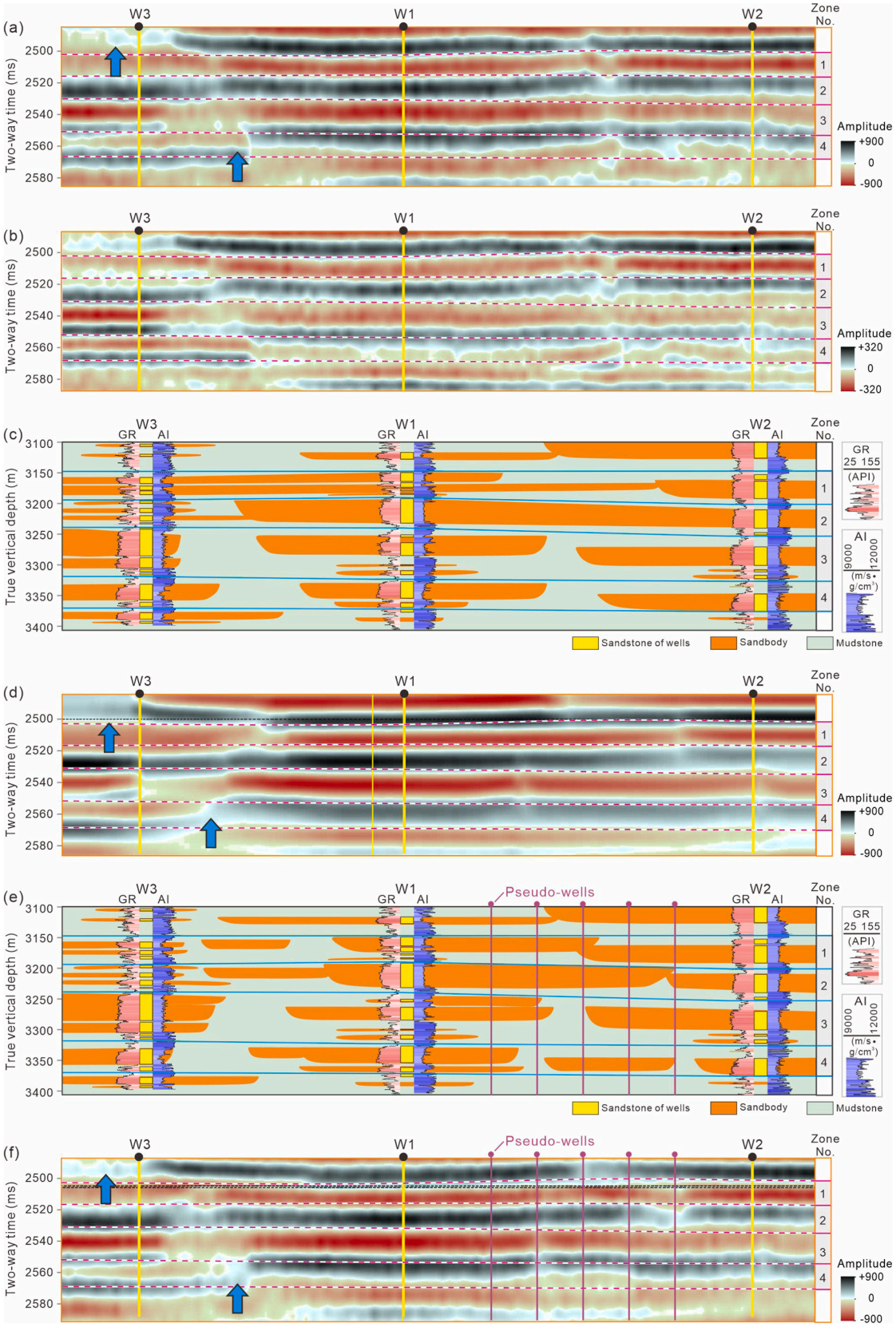

Fig. 9. Forward seismic modeling of a real well-correlation section. (a) and (b) are profiles of the original and high-frequency spectral-decomposed seismic data, respectively. The seismic reflections on these both profiles were flatten basing the top horizon of Zone 3, and performed smoothing. (c) Initial forward geological model. (d) Synthetic seismic reflection of the initial geological model. (e) Iteratively adjusted geological model. (f) Synthetic seismic reflection of the adjusted geological model. Forward seismic modeling is based on the concept of 'wave front sweep velocity', and was carried out in GeoGraphix Seismic Modeling (LMKR). Abbreviation: AI – acoustic impedance. Note: only five pseudo-wells are shown, by way of example.

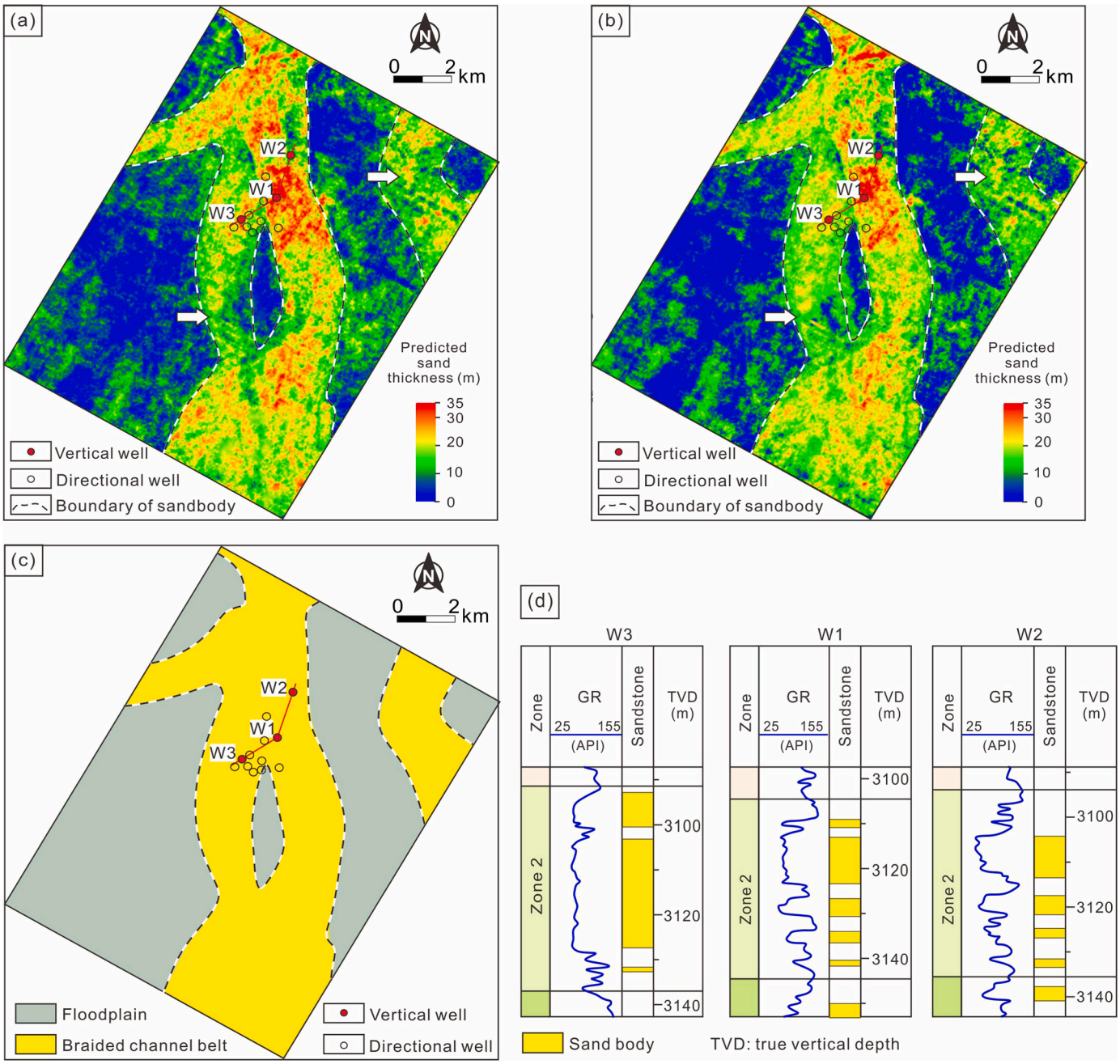

Fig. 10. Integrated attributes and predicted channel-belt sandbodies in reservoir zone 2. (a) Integrated attribute using the original MPA, RMS and sweetness attributes, derived by forward seismic modeling. (b) Integrated attribute using the high-frequency MPA, RMS and sweetness attributes. The integrated attribute represents a measure of predicted sand thickness. (c) Planform distribution of fluvial channel-belt sandbodies. (d) Well profiles of W1, W2, and W3, showing the wireline log of GR and lithological section.

(Fig. 11a).

Overall, the integrated seismic attribute obtained using the proposed method benefits from three significant advantages, compared to the original seismic attributes (Figs. 7, 10 and 11), as follows. (i) The proposed method results in improved correlation between seismic attribute and sand thickness, with a higher correlation coefficient (0.849 vs. 0.586; Fig. 11a and b). (ii) Channel belts can be more readily traced using the integrated attribute, than either using the original or high-frequency MPA attributes (Figs. 7 and 10a). In particular, some of the channel belts (indicated with arrows in Figs. 7 and 10a) are difficult to identify in the original attributes, whereas they are mapped clearly using the integrated attribute. (iii) The proposed method allows explicit prediction of sand thickness.

5.2. Application prospects

The integration of multiple seismic attributes with machine learning is an effective tool for attribute optimization, which has become increasingly popular in recent years (Anifowose et al., 2019; Li et al., 2020, 2021; Wang et al., 2020; Yue et al., 2019). However, application of this kind of method commonly hinges upon the availability of a dense array of wells that provide a training dataset for supervised machine learning, which greatly limits its application to fields with limited well control.

Due to the high drilling costs, offshore oilfields are often characterized by a limited number of drilled wells, commonly centered around a drilling planform (e.g., Fig. 2a). Therefore, established approaches to

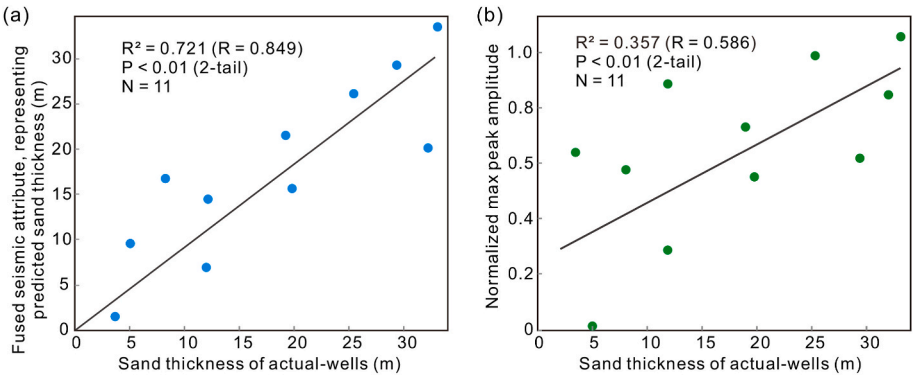

Fig. 11. Correlation analyses for zone 2 based on the 11 actual wells. (a) Relationship between observed sand thickness and integrated seismic attribute derived by forward seismic modeling. This integrated attribute is based on original MAP, RMS and sweetness attributes, corresponding to Fig. 10a. (b) Relationship between observed sand thickness and the original MPA attribute, corresponding to Fig. 7a. R^2 is the coefficient of determination; P-values report the statistical significance of correlations. Notably, the pseudo-wells were used in the supervised machine learning, whereas the actual wells are not used in the supervised machine learning.

seismic attribute optimization with supervised machine learning are not often applicable to offshore fields undergoing exploration or appraisal. Nonetheless, high-quality seismic data are commonly available in offshore fields, which hence represent an ideal setting for the application of the proposed method based on the generation of a training dataset to supervised machine learning using forward seismic modeling. Similarly, the proposed method can be widely applied in onshore fields undergoing exploration, and for which limited well data may exist.

5.3. Limitations

There are two main limitations in the use of the proposed method of seismic attribute optimization based on forward seismic modeling, related to the heterogeneity of the reservoirs and the complexity of the seismic data.

The approach relies crucially on sufficient similarity between the lithological model used for forward seismic modeling and the reservoir being studied, in terms of geometry, scale, density and stacking patterns of channel bodies (Stright et al., 2014; Tomasso et al., 2010). However, establishing a lithological model that adheres closely to the actual stratal architecture of the reservoir is not a trivial task, due to intrinsic reservoir heterogeneity (Li et al., 2020; Miall, 2006; Rafieepour et al., 2020; Zheng, 2018; Zheng et al., 2019). Therefore, the geological model used for forward seismic modeling must be realistic and contain appropriately simplified patterns. The bias in the forward geological model is also a potential limitation, because a well-correlation section occurs over a small area that may not be representative of the field as a whole.

The second main limitation is due to the used seismic wavelet and the complexity of the seismic data. To some degree, seismic wavelets can vary in space in the seismic data, but this information is not readily obtained (Hilterman, 1975). Hence, for simplicity, a uniform statistical wavelet extracted from the seismic data is used in the forward seismic modeling.

Nonetheless, the geological model and its synthetic seismic-reflection model are still reasonable and reliable, for the following reasons. First, the simplified lithological model shown in Fig. 9e is relatively high-resolution, compared to the low resolution of seismic data (0.25 wavelength is equal to 48 m). (ii) The seismic wavelet is not expected to change markedly in the same seismic dataset at comparable depths, justifying the use of a statistical wavelet extracted from the seismic data (Hilterman, 1975; Stright et al., 2014; Yue et al., 2019). (iii) Forward seismic modeling is effectively a primary seismic interpretation method, whose evaluation is rendered possible by using control wells to calibrate predictions of channel-body presence using integrated seismic attributes derived from forward seismic modeling.

6. Conclusions

1. A novel method of seismic attribute optimization supported by forward seismic modeling is proposed, which enables the integration of multiple attributes using supervised machine learning in fields with limited well control and improves the interpretation of seismic attributes. This method includes two main tasks: (i) forward seismic modeling of a well-correlation panel informed by seismic data, and (ii) fusing multiple seismic attributes by supervised machine learning using the forward seismic model as a training dataset.
2. Application of this method to a dataset consisting of 11 wells and a 3D seismic cube demonstrates that this approach to seismic attribute optimization is a new powerful predictive tool. Compared to the original seismic attributes, the integrated attribute produced by the proposed method allows direct prediction of sand thickness, returns a higher correlation between attribute and sand thickness, and results in clearer imaging of the planform distribution of channel-belt sandbodies.

Declaration of competing interest

The authors declare that they have no known competing financial interests or personal relationships that could have appeared to influence the work reported in this paper.

Data availability

Data will be made available on request.

Acknowledgements

This research is financially supported by the China Postdoctoral Program for Innovative Talents (BX20220351), the National Natural Science Foundation Project of China (42202109, 42272186), Project of RIPEO (2021DJ1101), Young Elite Scientist Sponsorship Program by Bast (BYESS2023460), Cooperation Project of the PetroChina Corporation (ZLZX 2020-02), and the China Postdoctoral Science Foundation (2022M713458, 2022M723489). LC thanks the sponsors of the Fluvial, Eolian & Shallow-Marine Research Group (AkerBP, Areva [now Orano], BHP, Cairn India [Vedanta], Chevron, CNOOC International, ConocoPhillips, Equinor, Murphy Oil, Occidental, Saudi Aramco, Shell, Tullow Oil, Woodside, and YPF).

References

Anifowose, F., Abdulraheem, A., Al-Shuhail, A., 2019. A parametric study of machine learning techniques in petroleum reservoir permeability prediction by integrating seismic attributes and wireline data. J. Pet. Sci. Eng. 176, 762–774. https://doi.org/10.1016/j.petrol.2019.01.110.

Armitage, D.A., Stright, L., 2010. Modeling and interpreting the seismic-reflection expression of sandstone in an ancient mass-transport deposit dominated deep-water slope environment. Mar. Petrol. Geol. 27, 1–12. https://doi.org/10.1016/j.marpetgeo.2009.08.013.

Bakke, K., Kane, I.A., Martinsen, O.J., Petersen, S.A., Johansen, T.A., Hustoft, S., Jacobsen, F.H., Groth, A., 2013. Seismic modeling in the analysis of deep-water sandstone termination styles. Am. Assoc. Petrol. Geol. Bull. 97, 1395–1419. https://doi.org/10.1306/03041312069.

Bitrus, P.R., Iacopini, D., Bond, C.E., 2016. Defining the 3D geometry of thin shale units in the Sleipner reservoir using seismic attributes. Mar. Petrol. Geol. 78, 405–425. https://doi.org/10.1016/j.marpetgeo.2016.09.020.

Castagna, J.P., Sun, S., 2006. Comparison of spectral decomposition methods. First Break 24, 75–79. https://doi.org/10.3997/1365-2397.24.1093.26885.

Chopra, S., Marfurt, K.J., 2005. Seismic attributes - a historical perspective. Geophysics 70. https://doi.org/10.1190/1.2098670, 3SO–28SO.

de Matos, M.C., Davogustto, O., Zhang, K., Marfurt, K.J., 2011. Detecting stratigraphic discontinuities using time-frequency seismic phase residues. Geophysics 76. https://doi.org/10.1190/1.3528758. P1–P10.

Eichelberger, N.W., Nunns, A.G., Groshong, R.H., Hughes, A.N., 2017. Direct estimation of fault trajectory from structural relief. Am. Assoc. Petrol. Geol. Bull. 101, 635–653. https://doi.org/10.1306/08231616065.

Hao, L., Wang, Q., Tao, H., Li, X., Ma, D., Ji, H., 2018. Geochemistry of oligocene Huagang Formation clastic rocks, Xihu sag, the East China Sea Shelf basin: provenance, source weathering, and tectonic setting. Geol. J. 53, 397–411. https://doi.org/10.1002/gj.2906.

Hart, B.S., 2008. Channel detection in 3-D seismic data using sweetness. Am. Assoc. Petrol. Geol. Bull. 92, 733–742. https://doi.org/10.1306/02050807127.

Hilterman, F.J., 1975. Amplitudes of seismic waves—a quick look. Geophysics 40, 745–762. https://doi.org/10.1190/1.1440565.

Hosseinyar, G., Moussavi-Harami, R., Abdollahie Fard, I., Mahboubi, A., Noemani Rad, R., 2019. Seismic geomorphology and stratigraphic trap analyses of the lower cretaceous siliciclastic reservoir in the kopeh dagh-amu darya basin. Petrol. Sci. 16, 776–793. https://doi.org/10.1007/s12182-019-0347-1.

La Marca, K., Bedle, H., 2022. Deepwater seismic facies and architectural element interpretation aided with unsupervised machine learning techniques: taranaki basin, New Zealand. Mar. Petrol. Geol. 136, 105427 https://doi.org/10.1016/j.marpetgeo.2021.105427.

Li, W., Yue, D., Colombera, L., Du, Y., Zhang, S., Liu, R., Wang, W., 2021. Quantitative prediction of fluvial sandbodies by combining seismic attributes of neighboring zones. J. Pet. Sci. Eng. 196, 107749 https://doi.org/10.1016/j.petrol.2020.107749.

Li, W., Yue, D., Wang, Wenfeng, Wang, Wurong, Wu, S., Li, J., Chen, D., 2019a. Fusing multiple frequency-decomposed seismic attributes with machine learning for thickness prediction and sedimentary facies interpretation in fluvial reservoirs. J. Pet. Sci. Eng. 177, 1087–1102. https://doi.org/10.1016/j.petrol.2019.03.017.

Li, W., Yue, D., Wu, S., Shu, Q., Wang, W., Long, T., Zhang, B., 2020. Thickness prediction for high-resolution stratigraphic interpretation by fusing seismic attributes of target and neighboring zones with an SVR algorithm. Mar. Petrol. Geol. 113, 104153 https://doi.org/10.1016/j.marpetgeo.2019.104153.

Li, W., Yue, D., Wu, S., Wang, Wenfeng, Li, J., Wang, Wurong, Tian, T., 2019b. Characterizing meander belts and point bars in fluvial reservoirs by combining spectral decomposition and genetic inversion. Mar. Petrol. Geol. 105, 168–184. https://doi.org/10.1016/j.marpetgeo.2019.04.015.

Mahob, P.N., Castagna, J.P., 2003. AVO polarization and hodograms: AVO strength and polarization product. Geophysics 68, 849–862. https://doi.org/10.1190/1.1581037.

McArdle, N.J., Iacopini, D., KunleDare, M.A., Paton, G.S., 2014. The use of geologic expression workflows for basin scale reconnaissance: a case study from the Exmouth Subbasin, North Carnarvon Basin, northwestern Australia. Interpretation 2, SA163–SA177. https://doi.org/10.1190/INT-2013-0112.1.

Miall, A.D., 2006. Reconstructing the architecture and sequence stratigraphy of the preserved fluvial record as a tool for reservoir development: a reality check. Am. Assoc. Petrol. Geol. Bull. 90, 989–1002. https://doi.org/10.1306/02220605065.

Naseer, M.T., Asim, S., 2017. Detection of cretaceous incised-valley shale for resource play, Miano gas field, SW Pakistan: spectral decomposition using continuous wavelet transform. J. Asian Earth Sci. 147, 358–377. https://doi.org/10.1016/j.jseaes.2017.07.031.

Partyka, G., Gridley, J., Lopez, J., 1999. Interpretational applications of spectral decomposition in reservoir characterization. Lead. Edge 18, 353–360. https://doi.org/10.1190/1.1438295.

Postnikov, E.B., Lebedeva, E.A., Lavrova, A.I., 2016. Computational implementation of the inverse continuous wavelet transform without a requirement of the admissibility condition. Appl. Math. Comput. 282, 128–136. https://doi.org/10.1016/j.amc.2016.02.013.

Rafieepour, S., Zheng, D., Miska, S., Ozbayoglu, E., Takach, N., Yu, M., Zhang, J., 2020. Combined experimental and well log evaluation of anisotropic mechanicalproperties of shales: an application to wellbore stability in bakken formation. In: SPE Annual Technical Conference and Exhibition. Virtual, pp. 1–20. https://doi.org/10.2118/201334-MS.

Sediek, O.A., Wu, T.Y., McCormick, J., El-Tawil, S., 2022. Prediction of Seismic collapse behavior of deep steel columns using Machine learning. Structures 40, 163–175. https://doi.org/10.1016/j.istruc.2022.04.021.

Shao, D.L., Fan, G.Z., Wang, H.Q., Ma, H.X., Zuo, G.P., Ding, L.B., Cai, Z., Li, W.Q., 2021. 3D anatomy and flow dynamics of net-depositional cyclic steps on the world's largest submarine fan: a joint 3D seismic and numerical approach. Petrol. Sci. 18, 10–28. https://doi.org/10.1007/s12182-020-00512-3.

Sinha, S., Routh, P.S., Anno, P.D., Castagna, J.P., 2005. Spectral decomposition of seismic data with continuous-wavelet transform. Geophysics 70, 19–25. https://doi.org/10.1190/1.2127113.

Stright, L., Stewart, J., Campion, K., Graham, S., 2014. Geologic and seismic modeling of a coarse-grained deep-water channel reservoir analog (Black's Beach, La Jolla, California). Am. Assoc. Petrol. Geol. Bull. 98, 695–728. https://doi.org/10.1306/09121312211.

Tomasso, M., Bouroullec, R., Pyles, D.R., 2010. The use of spectral recomposition in tailored forward seismic modeling of outcrop analogs. Am. Assoc. Petrol. Geol. Bull. 94, 457–474. https://doi.org/10.1306/08240909051.

Wang, X., Zhang, B., Zhao, T., Hang, J., Wu, H., Yong, Z., 2017. Facies analysis by integrating 3D seismic attributes and well logs for prospect identification and evaluation - a case study from Northwest China. Interpretation 5. https://doi.org/10.1190/INT-2016-0149.1. SE61–SE74.

Wang, Z., Gao, D., Lei, X., Wang, D., Gao, J., 2020. Machine learning-based seismic spectral attribute analysis to delineate a tight-sand reservoir in the Sulige gas field of central Ordos Basin, western China. Mar. Petrol. Geol. 113, 104136 https://doi.org/10.1016/j.marpetgeo.2019.104136.

Xu, F., Xu, G., Liu, Y., Zhang, W., Cui, H., Wang, Y., 2020. Factors controlling the development of tight sandstone reservoirs in the Huagang Formation of the central inverted structural belt in Xihu sag, East China Sea Basin. Petrol. Explor. Dev. 47, 101–113. https://doi.org/10.1016/S1876-3804(20)60009-X.

Yue, D., Li, W., Wang, W.W., Hu, G., Qiao, H., Hu, J., Zhang, M., Wang, W.W., 2019. Fused spectral-decomposition seismic attributes and forward seismic modelling to predict sand bodies in meandering fluvial reservoirs. Mar. Petrol. Geol. 99, 27–44. https://doi.org/10.1016/j.marpetgeo.2018.09.031.

Zeng, H., 2017. Thickness imaging for high-resolution stratigraphic interpretation by linear combination and color blending of multiple-frequency panels. T411————————T422 Interpretation 5. https://doi.org/10.1190/INT-2017-0034.1.

Zeng, H., Backus, M.M., 2005. Interpretive advantages of 90[degree]-phase wavelets: Part 2 — Seismic applications. Geophysics 70, C17–C24. https://doi.org/10.1190/1.1925741.

Zhang, B., Liu, Y., Pelissier, M., Hemstra, N., 2014. Semiautomated fault interpretation based on seismic attributes. Interpretation 2, SA11–SA19. https://doi.org/10.1190/INT-2013-0060.1.

Zheng, D., 2018. Experimental Study of Anisotropic Strength Properties of Shale. The University of Tulsa, ProQuest Dissertations Publishing.

Zheng, D., Miska, S., Ziaja, M., Zhang, J., 2019. Study of anisotropic strength properties of shale. AGH Drilling, Oil, Gas 36, 93–112.

Zheng, D., Ozbayoglu, E.M., Miska, S.Z., Liu, Y., 2022a. Cement sheath fatigue failure prediction by support vector machine based model. In: Paper Presented at the SPE Eastern Regional Meeting. Wheeling, West Virginia, USA, pp. 1–9. https://doi.org/10.2118/211880-MS.

Zheng, D., Ozbayoglu, E.M., Miska, S.Z., Liu, Y., Li, Y., 2022b. Cement sheath fatigue failure prediction by ANN-based model. Houston, Texas, USA. In: Paper Presented at the Annual Offshore Technology Conference, pp. 1–9. https://doi.org/10.4043/32046-MS.

Zhou, X., Xu, G., Cui, H., Zhang, W., 2020. Fracture development and hydrocarbon accumulation in tight sandstone reservoirs of the Paleogene Huagang Formation in the central reversal tectonic belt of the Xihu Sag, East China Sea. Petrol. Explor. Dev. 47, 499–512. https://doi.org/10.1016/S1876-3804(20)60068-4.